X-ray-absorption study of chemical short-range order in the amorphous $Fe_{40}Ni_{40}P_{14}B_6$ and $Co_{70}(Si,B)_{23}Mn_5(Fe,Mo)_2$ alloys

Peter Kizler

*Hamburger Synchrotronstrahlungslabor HASYLAB at the Deutsches Elektronen-Synchrotron DESY, Notkestrasse 85,
D-22607 Hamburg, Germany*

X-ray-absorption fine-structure data of the metal-absorption edges in the amorphous $Fe_{40}Ni_{40}P_{14}B_6$ and $Co_{70}(Si,B)_{23}Mn_5(Fe,Mo)_2$ alloys suggest segregation into microphases with different stoichiometric compositions; in the first case the material contains microphases consisting mainly of Ni and P and others of mainly Fe and B. The second material contains microphases with mainly Co-Si stoichiometry and a Mn-Fe-Mo-B mixture in the remaining part of the sample.

I. INTRODUCTION

The most intensively investigated amorphous alloys are of the type $T_{\sim 80}M_{\sim 20}$ with T being transition metals such as Mn, Fe, Co, or Ni and M metalloids like B, C, P, or Si. During the past years structural investigations have revealed several types of ordering in those alloys.

A. Topological short-range order

The atomic short-range order in amorphous alloys of the above type has been investigated by diffraction methods. Extensive neutron-diffraction experiments on amorphous $Ni_{75}P_{25}$,[1] $Fe_{75}P_{25}$,[2] $Fe_{80}B_{20}$,[3] $Ni_{81}B_{19}$,[4] and $Ni_{80}P_{20}$,[5] utilizing the isotopic substitution method have provided partial pair-correlation functions $G_{ij}(r) = 4\pi r[\rho_{ij}(r) - \rho_0]$, where $\rho_{ij}(r)$ is the partial atomic-density distribution function of the jth atom around the ith atom and ρ_0 is the average atomic density.

The shapes of the partial $G_{T-T}(r)$ curves for the different alloys are almost identical and there is also similarity between the $G_{T-M}(r)$ and $G_{M-M}(r)$ functions. Only the positions of the peak maxima of the $G_{ij}(r)$ functions differ slightly due to the differences in the atomic radii of the components. For the ternary $Fe_{40}Ni_{40}P_{20}$, $Fe_{40}Ni_{40}P_{14}B_{20}$, $Fe_{27}Ni_{50}B_{23}$, and the quaternary $Fe_{40}Ni_{40}P_{14}B_6$ alloys diffraction experiments show that for the alloys with more than two constituents the (total) pair-correlation functions are still very similar.[6,7] Therefore, as far as topological short-range order is concerned, in the $T_{80}M_{20}$ alloys the atoms always seem to be arranged according to the same geometrical principles. For the $Co_{70}(Si,B)_{23}Mn_5(Fe,Mo)_2$ alloy, which has not yet been investigated by diffraction methods, this is also expected to be true for the T-M and the paramount Co-Co pair correlations.

B. Chemical short-range order

For amorphous alloys of the $T_{80}M_{20}$ type, the partial $G_{PP}(r)$ or $G_{BB}(r)$ functions given in different publications[1–5] clearly demonstrate that the metalloid atoms

avoid direct contact and are exclusively bound to metal atoms, which is equivalent to the existence of a pronounced chemical short-range order. The short-range-order parameter defined by Cargill and Spaepen[8] characterizes the degree of a chemical order. Even for a metallic glass with a higher metalloid content, $Ni_{64}B_{36}$,[9] the partial coordination number N_{BB}, although greater than zero, was still smaller than in crystalline Ni_2B.[10] Once again it is expected that also in the $Fe_{40}Ni_{40}P_{14}B_6$ and in the $Co_{70}(Si,B)_{23}Mn_5(Fe,Mo)_2$ alloys direct metalloid-to-metalloid contact is avoided.

Despite the knowledge on chemical short-range order in the above binary amorphous alloys, little is known about preferred bonding in amorphous alloys with more than two constituents. Neutron-diffraction experiments on amorphous CoMnB alloys with isomorphic substitution[11] have demonstrated that B atoms are preferentially bound to Co and that Co-Mn pairs are preferred in comparison to Co-Co and Mn-Mn pairs. In the case of amorphous $(FeMn)_{75}P_{15}C_{10}$, however, no such ordering has been observed.[12] The structural relaxation resulting from annealing of $(Fe,Ni,Mn)_{80}B_{10}Si_{10}$ shows that Fe atoms may be replaced by Mn without essential structural changes, whereas replacing Fe by Ni leads to a somewhat different structure after relaxation.[13] Therefore chemical ordering in amorphous alloys with more than two constituents is not well understood and a direct structural probe would be very helpful, more especially since in amorphous alloys like $Fe_{40}Ni_{40}P_{14}B_6$ the metalloids strongly influence, for instance, the magnetic properties[14] and corrosion behavior.[15] An early indication of chemical ordering in amorphous $Fe_{40}Ni_{40}P_{14}B_6$ was derived from an investigation of the extended x-ray-absorption fine structure (EXAFS).[16] The different temperature dependence of the EXAFS amplitudes at the Ni- and Fe-K edge was explained in terms of different bond strengths between the Fe and Ni atoms and their local environment. Since a bond between Fe and Ni atoms would have to share the same mutual correlation function $G_{FeNi}(r)$, this difference in bond strengths can only be explained by a particular spatial segregation of Fe and Ni atoms. In a second EXAFS study evidence was again found for a so-

called microheterogeneous structure in the same alloy.[17] The data evaluation used in that work was based on the assumption of Gaussian radial density functions. This assumption, however, introduces problems into the data evaluation for highly disordered systems,[18] therefore, from these results only the existence of inhomogeneities can be derived. Any statement on their stoichiometry or internal structure is inconclusive. Finally, indications on the existence of two different types of Fe neighborhood in amorphous $Fe_{40}Ni_{40}P_{14}B_6$ were also derived from the alloy's magnetic properties[19] and from a Mössbauer study,[20] which demonstrated that besides the Fe-B neighborhood also a small fraction of Fe-P bondings must exist.

C. Modeling

Based on numerical data of the partial pair-correlation functions of binary amorphous alloys, three-dimensional structural models for the structure of such alloys have been generated successfully. Such models must be used, e.g., for the simulation of x-ray-absorption near-edge spectra (XANES).[21,22] A survey of models for amorphous $T_{80}B_{20}$ alloys is given in Ref. 23; for the amorphous $Fe_{80}P_{20}$ alloy only one model was reported in the literature.[24] For $Ni_{80}P_{20}$ a model was built[25] in agreement with diffraction data[5] using the simplified molecular-dynamics computer code of Brandt and Kronmüller.[26] Detailed geometrical studies of such structural models (e.g., Refs. 23, 24, and 27) made obvious that in amorphous alloys there is no single unique topological short-range order but a large variety of different individual short-range geometries, which, taken together, form an average topological short-range structure in an amorphous alloy.

D. Medium-range order

As well as short-range order, medium-range order can also be observed in amorphous alloys. Neutron small-angle scattering experiments have revealed the existence of inhomogeneities with a diameter of 1–2 nm in amorphous $Fe_{80}B_{20}$.[28] For $Ni_{80}P_{20}$ (Refs. 29 and 30) and $Fe_{40}Ni_{40}P_{20}$,[31] such inhomogeneities have been identified as fluctuations in the stoichiometric composition by a few atomic percent. X-ray small-angle scattering intensities obtained from amorphous $Fe_{40}Ni_{40}P_{14}B_6$ (Ref. 32) are unfortunately too low to decide clearly on the existence of such inhomogeneities in this case, but measurements with the Kerr effect[33] and Bitter technique[34] performed on $Fe_{40}Ni_{40}P_{14}B_6$ and $Co_{70}Fe_5Si_9B_{16}$ again demonstrate the existence of regions with internal stress and a diameter of approximately 3 μm. The structural models mentioned above are not able to incorporate such compositional fluctuations because the diameters of the models are too small. But the stoichiometrical fluctuation in the local environment between any atom and its neighbor[23] is larger than between the inhomogeneities (e.g., Refs. 29 and 30). Therefore, the existence of a medium-range order in the sense of a fluctuation in stoichiometry requires no more than a different weighting of local structural units in different areas of the bulk, not an essential

difference in the topological short ranges in the different inhomogeneities. Thus the principle of a topological network of structural units in the models is still valid.

II. X-RAY ABSORPTION SPECTROSCOPY: XANES AND EXAFS

X-ray-absorption fine structure (XAFS) is the modulation of the photoabsorption cross section due to the interference of the de Broglie wave of the ejected photoelectron with that which is backscattered by the surrounding atoms. The main advantage of this effect utilized as a structural probe is its selectivity to the neighborhood around the x-ray-absorbing atomic species. Both the XANES spectral range, for x-ray energies up to approximately 50 eV above the absorption edge, as well as the EXAFS, covering energies up to several hundred eV above the edge, are capable of revealing information related to different aspects of the structure.

A. The EXAFS range

Quantitative EXAFS data evaluation relies essentially on the analytical shape of the underlying radial distribution functions of the constituents.[35] For crystalline cases Gaussian radial distribution functions are a good approximation, however, for systems with large disorder, this expression as well as analytical asymmetrical radial distribution functions lead in numerous investigations to bond length or coordination numbers inconsistent with diffraction data.[36−38] Up to the present there is no general rule to overcome this difficulty,[18] nevertheless, some information can be derived from the EXAFS spectra of $Fe_{40}Ni_{40}P_{14}B_6$; further details are given in Sec. V.

B. The XANES range

In the XANES region the curved nature of the electron wave becomes important together with a small contribution from multiple scattering events. While EXAFS simply reflects the atomic distance and coordination number around the absorbing atom, XANES is sensitive to additional structural features. In particular:

XANES is sensitive to the location of atoms in a row between others, relative to its neighbors, in contrast to EXAFS, which is only sensitive to the location relative to the central atom, see, e.g., Sec. 2.4 in Ref. 39.

In the XANES region scattering angles of $0° < \vartheta < 180°$ gain importance, thereby making XANES sensitive to bond angles.[39,40]

Scattering amplitudes and phase shifts depend on the electron wave number k[41] as well as on the atomic number Z of the elements involved. The dependence is greater for low Z numbers and small k values, i.e., in the XANES region, than for heavier elements or for the EXAFS region.

Theoretical treatments and computer codes[40,42,43] permit XANES spectra to be simulated from structural data, even for amorphous alloys with a diversity of short-range

structures.[21,22] For the present work the ICXANES computer code of Vvedensky, Saldin, and Pendry[43] was used. Briefly, the electron transition rate is calculated within the dipole approximation, using essentially an atomic contribution modified by single and multiple scattering of the excited electron by the surrounding atoms. The scattering property of each atom is characterized by the phase shifts δ_l for incident spherical waves of angular momentum l. The required phase shifts are calculated by integration of the Schrödinger equation using the program MUFPOT[44] assuming a muffin-tin form for the atomic potentials in the bulk, obtained by the superposition of neutral atomic charge densities.[45] The phase shifts as well as structural data form the input to ICXANES, which provides the final simulated XANES curves.

Figure 1 demonstrates the angular-dependent scattering amplitudes of B, P, and Fe in the crystalline reference materials. They were calculated from the scattering phase shifts with the equation,[46]

$$|f(\Theta)| = k^{-1} \sum_{l=0}^{\infty} (2l+1) e^{i\delta_l} \sin\delta_l P_l(\cos\Theta) \ .$$

Scattering angles of 0° and 180° correspond to forward- and back-scattering, which are the dominating scattering processes in the EXAFS region. Angles between 0° and 180°, mainly around 120°, permit multiple-scattering processes on triangular or other looped paths. The scattering behavior differs drastically among the elements. P possesses a very strong forward scattering power and, contrary to the other elements, its backscattering power raises with increasing energy. Surprisingly, the scattering power of the light B atoms competes well with the heavier iron. For the discussions in Secs. 7–9, it is important to realize that P as a scattering atom influences the XANES spectrum in quite a different way than a B atom does.
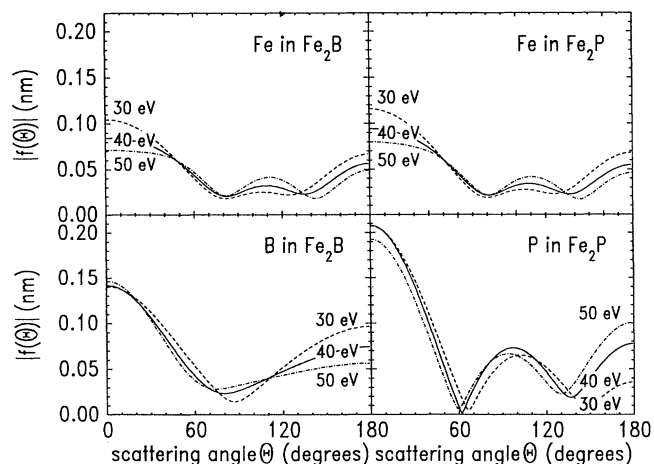
FIG. 1. Electron-scattering amplitudes $f(\theta)$ for B, P, and Fe in crystalline reference compounds, calculated for different electron energies.

III. MATERIALS

For the present work the following materials were investigated:

Amorphous alloys: $Fe_{40}Ni_{40}P_{14}B_6$ and $Fe_{80}B_{20}$, produced by the planar flow cast method and purchased as Metglas 2628 and 2605 from Allied Corp., Parsippany, New Jersey. The $Fe_{80}B_{20}$ sample was thinned for the EXAFS measurements with a sputtering device operated in the etching mode.

$Ni_{80}B_{20}$ was sputtered onto a water-cooled Mylar foil in a rf sputtering device; $Fe_{80}P_{20}$ and $Ni_{80}P_{20}$ were produced by electrodeposition[47] and made available by G. Dietz, University of Köln.

$Co_{70}(Si,B)_{23}Mn_5(Fe,Mo)_2$, prepared by melt spinning was produced by Vacuumschmelze Hanau (Germany) and purchased from Goodfellow Metals, Cambridge, (UK). A quantitative analysis was not performed by the manufacturer. Samples were thinned for XAFS measurements by mechanical polishing.

X-ray-diffraction diagrams to check for the amorphous state have partly been printed elsewhere.[48]

Crystalline reference samples: Fe_2B: The sample was prepared molten in an electron-beam furnace, from ingots of the pure elements. A powder sample was obtained afterwards by ball-milling. Powdered Ni_2P was purchased from A. D. Mackay Chemical Corp.

IV. MEASUREMENTS

The x-ray-absorption measurements (XAS) were performed in transmission mode at liquid-nitrogen temperature at the stations EXAFS II (Mn edge) and RÖMO II (all other edges) at the Hamburger Synchrotron-strahlungslabor HASYLAB at the Deutsches Elektronen-Synchrotron DESY. The intensities before and behind the sample were detected with nitrogen-filled ionization chambers. EXAFS II employs a focusing double-crystal monochromator using Si(111) crystals. The double-crystal monochromator RÖMO II was equipped with Si(311) crystals. A feedback control system for detuning the monochromator[49] served for suppression of higher harmonics in the monochromatic beam. Both monochromators achieve an energy resolution of $\Delta E < 1$ eV except for the Mo-K edge where ΔE was ≈ 4 eV.

V. EXAFS RESULTS

A. EXAFS data processing

From the absorption data Fourier-filtered EXAFS spectra of the first coordination sphere were extracted using a standard EXAFS data evaluation program package.[50] For the example of $Ni_{80}P_{20}$, Figs. 2(a)–2(c) and 3 demonstrate the single steps of data processing. Figure 2(b) shows the EXAFS oscillation as extracted from the raw data of Fig. 2(a). Figure 2(c) displays the Fourier transform obtained from the data of Fig. 2(b), convoluted with a Kaiser-Bessel window to minimize truncation effects. The backtransform of the data of Fig. 2(c) from the main peak, i.e., from the interval between $r = 0.9$ Å

and $r = 3.0$ Å is displayed in Fig. 3, together with its envelope curves. As is typical for amorphous alloys with their large static disorder, the Fourier transform consists of a main peak related to the first coordination sphere and of negligible contributions from more distant shells. In Fig. 3 the EXAFS spectra for the Fe and Ni edges in the quarternary $Fe_{40}Ni_{40}P_{14}B_6$ alloy are compared to those of the corresponding binary amorphous alloys. The data have been obtained from the EXAFS data by a Fourier transform of always the same k interval, followed by a backtransform of the same r interval as mentioned before in each case. The EXAFS data and amplitudes of
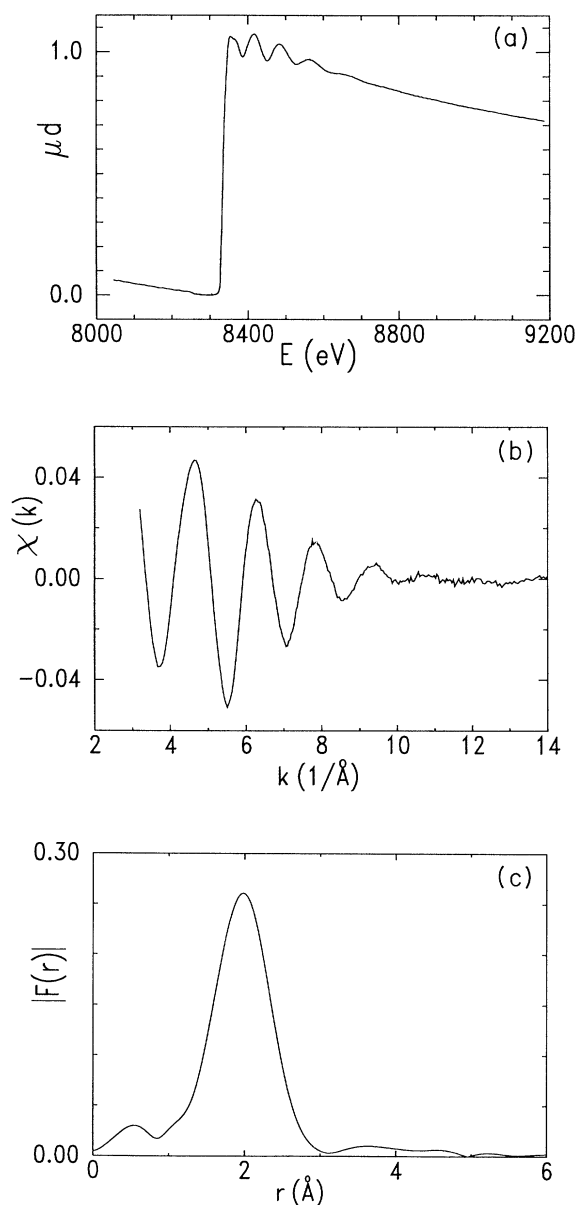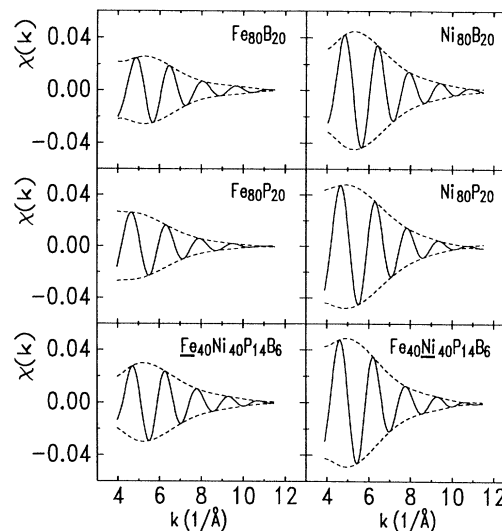
FIG. 3. Fourier-filtered (backtransformed) EXAFS curves of several amorphous $T_{80}M_{20}$-type alloys. Dashed lines: Envelopes.

the binary alloys are in very good agreement with already published equivalent data,[36,37] reported by different authors from different laboratories. This conformity among different measurements together with the negligible dependence of the structure on the method of preparation[38] makes the basis yet more reliable for the conclusions later on.

B. EXAFS results for $Fe_{40}Ni_{40}P_{14}B_6$

As was mentioned already, EXAFS data evaluation for amorphous materials is burdened with different difficulties, which are mainly the necessity of knowing in advance the shape of the radial distribution function and, in the present case, also the lack of knowledge on the contribution of metalloid EXAFS to the total spectrum.

Instead of dropping the less promising numerical EXAFS data evaluation, in the present peculiar case, new conclusions can be drawn. Admittedly, the sequence of arguments such as those utilized later on can only lead to solutions for rare, selected cases, and cannot serve as a general recipe for EXAFS studies. Briefly, some approved data shall be recalled:

(i) Theoretical calculations yielded backscattering amplitudes of Fe and Ni, which are almost identical;[51] see Fig. 4.

(ii) The metalloid atoms contribute only poorly to the total EXAFS spectrum, first due to their small atomic fraction (20%), second, due to their small backscattering amplitude over the major k range, especially for medium or higher k values; see Fig. 4.

(iii) Partial bond lengths and coordination numbers of all binary amorphous alloys consisting of the $T_{80}M_{20}$ type are almost identical[2-5] and therefore not responsible for possible large differences in EXAFS amplitudes.

(iv) The same is true for the comparison between the total coordination numbers and diffraction-peak radii of the quaternary $Fe_{40}Ni_{40}P_{14}B_6$ alloys and its binary rela-

FIG. 2. EXAFS data of amorphous $Ni_{80}P_{20}$ in different stages of data processing; (a) raw absorption data; (b) EXAFS oscillation; (c) Fourier transform of EXAFS data of Fig. 2(b). Backtransform from the main peak in Fig. 2(c): see Fig. 3.
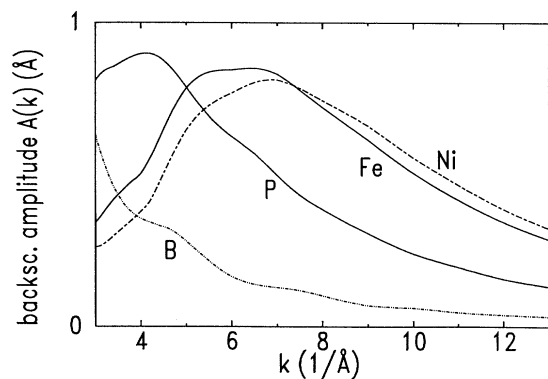
FIG. 4. Backscattering amplitudes as calculated by McKale *et al.* (Ref. 51) for B, P, Fe, and Ni.

FIG. 5. Direct comparison of the Ni EXAFS curves of Fig. 3; Continuous line: $Fe_{40}Ni_{40}P_{14}B_6$; dashed line: $Ni_{80}P_{20}$; dash-dotted line: $Ni_{80}B_{20}$.

tives. Since the atomic scattering factors of the metalloid atoms are smaller than those of the metals, the diffraction results of the quaternary alloy can nicely be compared to the metal-metal correlation data of the binary alloys and agreement in numerical values can be stated again. Moreover, due to the necessities of dense filling of space, without voids, the coordination number can hardly be different from what is known from diffraction studies.

The experimental data have to be discussed from this background. The common observation from Fig. 3 is that the amplitudes of all Ni spectra are considerably larger than those of the Fe edges, as was described already for amorphous $Fe_{40}Ni_{40}B_{20}$.[37] As was discussed in (ii) above these EXAFS curves reflect dominantly the metal-metal correlation function. The metal-metal coordination numbers cannot be considered responsible for such differences (iii), therefore the reason must result from the differences in width of the radial distribution functions. The data suggest that they are sharper for Ni-Ni pairs than for Fe-Fe pairs, independent of the kind of metalloid involved. This is in agreement with an investigation of the vibrational spectra of amorphous alloys[52] where a stronger interatomic force was found between Ni atoms than between Fe atoms. EXAFS data of crystallized materials, however, are severely different in amplitude and frequency composition,[36] and very sensibly detect the onset of structural changes towards crystalline order or precursors of order;[53] therefore the detected differences cannot be interpreted by crystallization phenomena.

In Fig. 5, a comparison of all Ni EXAFS data demonstrates an almost perfect coincidence. Only for small k values does the envelope of the $Ni_{80}B_{20}$ curve differ from the others, and this can be explained by the different backscattering amplitudes of B and P; see Fig. 4. Since the backscattering amplitudes of Fe and Ni are very similar similar and since a Ni-Fe bond would obviously imply a somewhat broader radial distribution function, the coincidence between the EXAFS curves of Ni in $Fe_{40}Ni_{40}P_{14}B_6$ and $Ni_{80}P_{20}$ suggests that Ni atoms have almost exclusively Ni atoms as metallic neighbors. For Fe the situation is less clear. The Fe EXAFS of $Fe_{40}Ni_{40}P_{14}B_6$ is neither identical to the results for $Fe_{80}B_{20}$, nor to those for $Fe_{80}P_{20}$, nor to a superposition
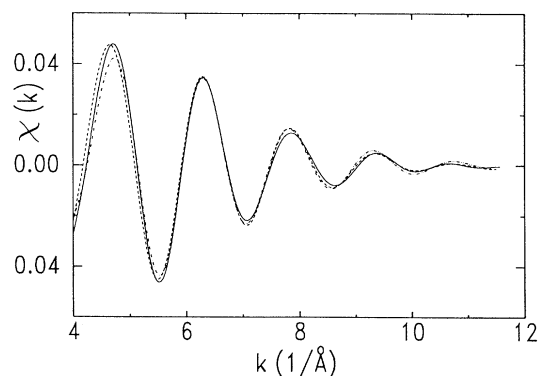
of both. Therefore the radial distribution function around Fe is somewhat different from that in the case the binary alloys. But, as in the case of Ni EXAFS, the Fe atoms seem to have an atomic neighborhood of dominantly the same chemical identity.

Due to the small backscattering amplitudes of B and P in the relevant k range conclusions on the metalloid environment of the metal atoms cannot be made.

VI. ESTIMATION OF THE MINIMUM SIZE OF THE MICROPHASES

Since the Fe- and Ni-EXAFS amplitudes in $Fe_{40}Ni_{40}P_{14}B_6$ differ considerably, most Fe or Ni atoms cannot share the same pair-correlation function G_{FeNi}, which means they cannot be neighbors and must therefore be part of Fe-rich and Ni-rich microphases. The term "phase" in the present context is not used in the rigid metallurgical sense of thermodynamically stable phase with well-defined structure. From the number of atoms located at the interface between the two hypothetical microphases their minimum size can be estimated.

For the sake of simplicity a small cube of 27 Ni atoms having the NaCl structure is assumed. Each face of the cube is covered by 9 Ni "interface" atoms, a total of 54 atoms, which, together with the bulk ones, yields 81 atoms. If this microphase were embedded in Ni, all those atoms would be able to yield 81 times a Ni-Ni EXAFS spectrum originating from their first neighbor shell. The estimation continues with further simplifications:

This Ni microphase is embedded in Fe of the same NaCl structure, i.e., the second microphase. This means that each Ni interface atom has 3.67 Ni and 2.33 Fe neighbors on average.

The partial pair-correlation function G_{FeNi} between Fe and Ni remains broadened, as in the case of the Fe-Fe bond.

An EXAFS curve caused by backscattering Fe atoms is roughly equivalent to a Ni spectrum reduced by 40%; see Fig. 3.

All Ni atoms together, bulk and interface, experience

only 72.5 times a Ni spectrum. This is a reduction of 10% as compared to the former 81 times for Ni embedded in Ni. Such a difference would be obvious in the Ni EXAFS of Ni in $Fe_{40}Ni_{40}P_{14}B_6$ and Ni in $Ni_{80}P_{20}$. Therefore, the minimum diameter of such Ni-rich microphases is that of the present example, 1 nm. The present estimation, however, does not distinguish between the case where there is a coexistence of microphases of similar shape in the bulk, or if one microphase is a host matrix with microphases of the other kind embedded, or which of the microphases is the host. Even for the binary amorphous $Ni_{80}P_{20}$ alloy this is still a matter of controversy.[29,30]

VII. XANES RESULTS FOR $Fe_{40}Ni_{40}P_{14}B_6$: EXPERIMENTAL DATA

Figure 6 shows experimental XANES data, together with simulated curves, which will be discussed in Sec. VIII. The data were obtained from the raw absorption data after subtracting the pre-edge absorption using a standard Victoreen fit.

Most obvious is the difference between the $T_{80}B_{20}$ and the $T_{80}P_{20}$ XANES data. Unlike the differences in the EXAFS case, essentially the difference in amplitudes, for the XANES parts completely different curve shapes are observed. Such a systematic difference calls for an exact interpretation and may be capable of bias suggestions
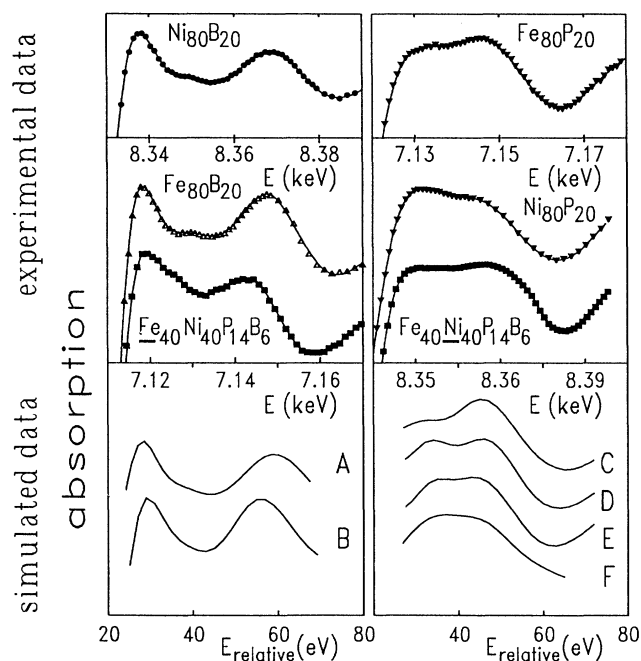
FIG. 6. Experimental and simulated XANES data and different alloys of the $T_{80}M_{20}$ types. Curves A–F: numerical XANES simulations. Curve A: model $Ni_{80}B_{20}$, wave functions Ni and B; Curve B: model $Ni_{80}P_{20}$, wave functions Ni and B; Curve C: model $Ni_{80}P_{20}$, wave function; Fe and P; Curve D: model $Ni_{80}P_{20}$, wave functions Ni and P; Curve E: model $Ni_{80}P_{20}$ with different interatomic potentials than model of curve D, wave functions Fe and P; Curve F: model $Ni_{80}B_{20}$, wave functions Fe and P. For details, see text.

about chemical short-range order even more striking than the EXAFS data do. In agreement with Fig. 1, B and P atoms exhibit different scattering behavior from electrons and a different energy dependence. The slopes of the XANES curves beyond the first peak do not differ for $Ni_{80}B_{20}$ and $Fe_{80}B_{20}$, whereas those for $Ni_{80}P_{20}$ and $Fe_{80}P_{20}$ do, although maintaining their general shape. Due to its small size and number of electrons, boron contributes little to the scattering processes, as has been demonstrated by numerical XANES calculations for amorphous $T_{80}B_{20}$ (Ref. 21) and for crystalline Fe_2B alloys.[39] Phosphorus, however, is capable of inducing stronger charge transfer and hybridization and therefore a more pronounced change in scattering behavior. A thorough theoretical study of charge transfers and hybridization of electronic levels in $-B_{20}$ and $-P_{20}$ alloys has already been performed,[54] and the different electronic behavior between crystalline Ni_2P and Fe_2P alloys has also been explained by means of electronic structure calculations.[55]

As far as the quaternary alloys are concerned, the striking similarity between the Ni XANES data and the binary $-P_{20}$ alloys is obvious as is the poorer correspondence between the Fe edge data and the binary $-B_{20}$ alloys. As was shown in Ref. 20, a small fraction of Fe-P bondings still has to be assumed. In both cases XANES data in the quaternary alloys show a contraction (for Fe) or an expansion (for Ni) of the features as a function of energy as compared to the binary counterparts. Such distortions can be ascribed to distortions of the bond lengths.[39,56]

As was mentioned in Sec. V, the EXAFS spectra relate only to atoms in the first coordination sphere. XANES spectra, however, incorporate scattering effects from atoms beyond the first coordination sphere and thus the detection of structural disortions does not contradict earlier conclusions from Sec. V where the short-range order in the first coordination sphere around Ni in the quaternary and binary alloys was found to be almost identical.

VIII. XANES RESULTS FOR $Fe_{40}Ni_{40}P_{14}B_6$: NUMERICAL SIMULATIONS

In order to separate the dependence of the XANES spectra from topological effects and chemical short-range order numerical XANES simulations were performed. Before such calculations can be performed for amorphous materials, the calculations must be verified for crystalline materials with a known structure. Thus XANES spectra of the crystalline alloys Fe_2B (Refs. 21 and 39) and Ni_2P (Ref. 57) were calculated with the requirement of convergence in cluster size, number of phase shifts, and electron damping. Using the verified input data, XANES calculations could be made exploiting coordinates of structural models for amorphous alloys; for details of the procedure see Refs. 21 and 22.

A. Calculation of XANES spectra from structural models

Curve A in Fig. 6 was calculated[21,22] for $Fe_{80}B_{20}$ and $Ni_{80}B_{20}$ alloys based on the structural model of Dubois,

Gaskell, and LeCaër.[58] Very good agreement between simulation and experiment was found. For the $Fe_{80}P_{20}$ and $Ni_{80}P_{20}$ alloys a new structural model has been generated using the computer code of Brandt.[26] The partial pair-correlation functions of this model agree very well with the experimental data for $Ni_{80}P_{20}$.[5] As a result of the experience with models for the $Ni_{80}B_{20}$ and $Fe_{80}B_{20}$ alloys[22,23] and the minor differences between the diffraction results for $Ni_{80}P_{20}$ (Ref. 5) and $Fe_{80}P_{20}$,[2] this model was treated as equivalent for Fe- and Ni-P alloys. Curves C and D are XANES results for the $Ni_{80}P_{20}$ model; D was calculated starting from Ni and P wave functions, while for curve C Fe wave functions were used. Whereas for $Fe_{80}B_{20}$ and $Ni_{80}B_{20}$ neither experiment nor calculation yields any significant difference,[21] for the $-P_{20}$ alloys the calculation correctly reproduces the difference in the slopes for the Ni and Fe cases. Further, the energy interval between maxima and minima in the data is reproduced correctly with only the agreement in the general slopes being not quite perfect. It was already apparent, however, that in the case of the $Fe_{80}B_{20}$ alloys the XANES simulations based on the Brandt model did not yield the best possible result,[22] and there is thus an inherent failing in the modeling strategy. This error is, however, not too grave in the present context. The only published structural model for $Fe_{80}P_{20}$ (Ref. 24) led to a less satisfying result and was therefore abandoned.

Using Brandt's computer code once more, a second structural model was constructed, for which the interatomic attractive and repulsive potentials were changed to obtain a different equilibrium and free-energy minimization in the structure. By this means it was possible to obtain partial pair-correlation functions from the model which were almost identical to the ones obtained previously. Curve E in Fig. 6 is the XANES result obtained from this alternative model. Despite the good agreement between the partial pair-correlation functions from model and experiment, there is now a poorer agreement between experimental and simulated data. This example demonstrates that changes in the XANES spectrum are not necessarily dependent on significant changes in interatomic distances but may arise from small variations in the interatomic bonds and thus from a change in the local geometries. The discrepancy between the XANES data for quaternary and binary alloys therefore does not suggest major structural changes but only subtle differences in short-range order.

B. Distinguishing between differences in topological and chemical short-range order

The foregoing hypothesis of preferential bonding of Ni to P and of Fe to B can be verified by XANES simulations. For this purpose the simulations for the $Ni_{80}P_{20}$ model were repeated using the phase shifts of the Fe-B system, see curve B. Similarly, the calculations for the $Ni_{80}B_{20}$ model were repeated using the phase shifts for the Ni-P system, resulting in curve F. Despite the "wrong" phase shifts for both permutations there is close similarity between experimental and simulated curves, which means that only the alloying metalloid atom, i.e.,

chemical short-range order, is responsible for the difference between the general shapes of the curves. It is interesting to note that the shapes of the calculated curves $(A-F)$ are already reproduced fairly well by a curved wave single-scattering calculation, which can be run with the same computer code. This means that already the backscattering behavior of the metalloid atoms, see "180°" values" in Fig. 1, is most responsible for the XANES curve shape. Such single-scattering results have already been published for $Fe_{80}B_{20}$.[22]

The conclusions can be summarized as follows:

Curve shape like A or B ↔ chemical short-range order: B as metalloid environment;

curve shape like C, D, E, or F ↔ chemical short-range order: P as metalloid environment;

difference between A and B ↔ difference of topological short-range order due to the different size of the metalloid atoms;

difference between C, E, and F ↔ difference of topological short-range order due to the different size of the metalloid atoms;

difference between C and D ↔ Ni instead of Fe atoms.

IX. XANES RESULTS FOR $Co_{70}(Si,B)_{23}Mn_5(Fe,Mo)_2$

In contrast to the case of the amorphous Ni-based alloys, the EXAFS amplitudes for Co-based amorphous alloys are quite similar to those of Fe-based alloys; see Ref. 59. Analysis of the EXAFS in this case is inconclusive and thus will not be treated further here.

The XANES data are shown in Fig. 7, and, although somewhat noisy, they are still sufficient for present purposes. Since Si and P are neighbors in the periodic system, their electron-scattering behavior is very similar and the phenomena ascribed to the P environment as discussed in Sec. VIII are transferable to the Si case.

A comparison between the experimental data of Figs. 6
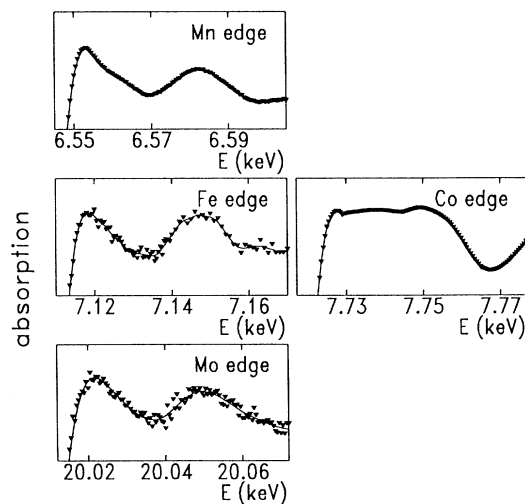
FIG. 7. Experimental XANES data of the metals in the amorphous $Co_{70}(Si,B)_{23}Mn_5(Fe,Mo)_2$ alloy.

and 7 illustrates for the Co edge again the typical P or Si shape and for the other metals' edges a close similarity to the Boron XANES curves of Fig. 6. If Co atoms have almost exclusively Si atoms as metalloid neighbors, thereby effectively excluding other metal atoms, then again a microphase segregation exists consisting of Co-Si-rich regions and other regions consisting of the remaining atoms. This alloy consists of six different chemical elements as compared to four in the previous example, and therefore the electron structure and the electron-scattering processes are even more complex. The remaining discrepancies between the XANES data of Figs. 6 and 7 are therefore not too surprising. The scattering behavior of Mn, Fe, and Mo does not differ too much, and thus the identity of the metal-metal environment does not influence the XANES spectra to a large extent. There is therefore a strong similarity in the XANES data for Mn, Fe, and Mo due to the absence of Si.

In the present context a suggested microphase segregation in amorphous $Co_{72.8}Fe_{5.2}Si_{11}B_{11}$ alloy as derived from the magnetic properties[60] provides an interesting analogy.

X. CONCLUSIONS

In the present paper chemical short-range order in the amorphous $Fe_{40}Ni_{40}P_{14}B_6$ and $Co_{70}(Si,B)_{23}Mn_5(Fe,Mo)_2$ alloys has been detected utilizing x-ray-absorption spectroscopy. In the case of $Fe_{40}Ni_{40}P_{14}B_6$ both the EXAFS and the XANES range provided useful information.

From EXAFS data the existence of chemical short-range order amongst the metal atoms could be derived, with the bulk segregated into microphases of Fe-rich and Ni-rich stoichiometry.

XANES data, on the other hand, has provided information on chemical short-range order between metal and metalloid atoms, and suggested that there is preferential chemical bonding between Ni and P as well as between Fe and B. This chemical short-range order implies the segregation of the alloy into Fe-rich and Ni-rich micro-phases as already made evident from the EXAFS results.

In the case of $Co_{70}(Si,B)_{23}Mn_5(Fe,Mo)_2$ it was possible from the XANES data to derive a microphase segregation into Co-Si-rich regions and regions consisting mainly of the remaining atomic species.

The suggested microphases agree generally with results on the same and related materials obtained by other experimental methods.

XANES spectra are frequently used as "fingerprints" for the identification of phases and geometrical structures in materials. This procedure is justified as long as the x-ray-absorbing species and its neighbors are identical or at least similar in both the unknown structure and the model compounds. It must be kept in mind that possibly different geometrical structures may cause the same XANES spectrum. The present results demonstrate, however, that, in certain cases, rather than topological effects, the chemical short-range order can have the major influence on the XANES data.

Since the differences in scattering behavior are more pronounced between lighter elements such as B and P than between heavier elements, for example, the $3d$ and $4d$ elements, the exploitation of these differences offers interesting new applications for XANES studies on complex systems.

[1]J. F. Sadoc and J. Dixmier, Mater. Sci. Eng. **23**, 187 (1976).

[2]Y. Waseda, H. Okazaki, and T. Masumoto, Sci. Rep. Res. Inst. Tohoku Univ. Ser. A **26**, 202 (1977).

[3]E. Nold, P. Lamparter, E. Olbrich, G. Rainer-Harbach, and S. Steeb, Z. Naturforsch. Teil A **36**, 1032 (1981).

[4]P. Lamparter, W. Sperl, S. Steeb, and J. Blétry, Z. Naturforsch. Teil A **37**, 1223 (1982).

[5]P. Lamparter and S. Steeb, in *Proceedings of the 5th International Conference on Rapidly Quenched Metals (RQ5)*, edited by S. Steeb and H. Warlimont (North-Holland, Amsterdam, 1985), p. 459.

[6]B. J. Thijsse and I. Majewska-Glabus in *Proceedings of the 5th International Conference on Rapidly Quenched Metals (RQ5)* (Ref. 5), p. 435; I. Siestsma and C. van Dijk, *ibid.*, p. 463; E. Svab, R. Bellissent, and G. Meszaros, *ibid.*, p. 467; Y. Egami, R. S. Williams, and Y. Waseda, in *Proceedings of the 3rd International Conference on Rapidly Quenched Metals*, edited by B. Cantor (Sussex University Press, Sussex, England, 1978), Vol. II, p. 318.

[7]E. Svab, N. Kroo, S. N. Ishmaev, I. P. Sadikov, and A. A. Chernyshov, Solid State Commun. **46**, 351 (1983).

[8]G. S. Cargill III and F. Spaepen, J. Non-Cryst. Solids **43**, 91 (1981).

[9]N. Cowlam, W. Guoan, P. O. Gardner, and H. A. Davies, J. Non-Cryst. Solids **61&62**, 337 (1984); S. N. Ishmaev, S. L. Isakov, I. P. Sadikov, E. Sváb, L. Kõszegi, A. Lovas, and G. Mészáros, *ibid.* **61&62**, 11 (1987).

[10]K. Schubert, *Kristallstrukturen zweikomponentiger Phasen* (Springer, Berlin, 1964).

[11]M. Heckele, P. Lamparter, S. Steeb, and R. Bellissent, Z. Naturforsch. Teil A **44**, 495 (1989).

[12]C. Janot, B. George, C. Tête, A. Chamberod, and J. Laugier, J. Phys. **44**, 1223 (1985); J. Phys. (Paris) Colloq. **46**, C8-143 (1985).

[13]R. Brüning, Z. Altounian, and J. O. Ström-Olsen, J. Appl. Phys. **62**, 3633 (1987).

[14]See, for example, C. L. Chien, D. Musser, F. E. Luborsky, and J. L. Walter, Solid State Commun. **28**, 645 (1978).

[15]H. Viefhaus, R. Möller, and M. Janik-Czachor, Werkst. Korros. **39**, 453 (1988).

[16]J. Wong, in *Glassy Metals,* edited by H. J. Güntherodt and H. Beck (Springer, Berlin, 1981), Vol. I, p. 67.

[17]E. Zschech, W. Blau, K. Kleinstück, H. Hermann, N. Mattern, M. A. Kozlov, and M. A. Sheromov, J. Non-Cryst. Solids **86**, 336 (1986).

[18]E. D. Crozier, J. J. Rehr, and R. Ingalls, in *X-Ray Absorption Spectroscopy,* edited by D. C. Koningsberger and R. Prins (Wiley, New York, 1988), Chap. 9.

[19]R. Höhne, H. C. Semmelhack, and G. Dietzmann, Exp. Tech. Phys. **19**, 365 (1971).

[20]K. Melzer, R. Höhne, E. Wieser, W. Matz, and B. Springmann, Nucl. Instrum. Methods Phys. Res. **199**, 169 (1982).

[21]P. Kizler, Ph.D. thesis, University of Stuttgart, 1988.

[22]P. Kizler, P. Lamparter, and S. Steeb, Z. Naturforsch. Teil A **44**, 189 (1989).

[23]P. Kizler, P. Lamparter, and S. Steeb, Z. Naturforsch. Teil A **43**, 1047 (1988).

[24]T. Fujiwara and Y. Ishii, J. Phys. F **10**, 1901 (1980).

[25]P. Kizler (unpublished).

[26]E. H. Brandt and H. Kronmüller, J. Phys. F **17**, 1291 (1987).

[27]See, for example, D. S. Boudreaux and H. J. Frost, Phys. Rev. B **23**, 1506 (1981); F. Lançon, L. Billard, and C. Chamberod, J. Phys. F **14**, 579 (1984).

[28]E. Nold, S. Steeb, P. Lamparter, and G. Rainer-Harbach, J. Phys. (Paris) Colloq. **41**, C8-186 (1980); P. Lamparter, S. Steeb, D. M. Kröger, and S. Spooner, in *Proceedings of the 6th International Conference on Rapidly Quenched Metals (RQ6),* edited by R. W. Cochrane and J. O. Ström-Olsen [Mater. Sci. Eng. **97**, 227 (1988)].

[29]K. Schild, F. Frisius, P. Lamparter, and S. Steeb, Z. Naturforsch. Teil A **40**, 551 (1985).

[30]R. Sonnberger, E. Pfanner, and G. Dietz, Z. Phys. B **63**, 203 ' (1986).

[31]A. R. Yavari, D. Bijaoui, M. C. Bellissent, P. Chieux, and M. Harmelin, in *Amorphous Metals,* edited by A. Hernando *et al.* (Elsevier, Amsterdam, 1987), p. 336.

[32]N. Mattern, J. Henke, M. Reibold, and H. Hermann, Phys. Status Solidi A **100**, 37 (1987).

[33]G. Dietz, J. Magn. Magn. Mater. **6**, 47 (1977); H. Kronmüller, R. Schäfer, and G. Schröder, *ibid.* **6**, 61 (1977); A. Hubert, *ibid.* **6**, 38 (1977); B. Gröger and H. Kronmüller, *ibid.* **9**, 203 (1978); G. Schröder, R. Schäfer, and H. Kronmüller, Phys. Status Solidi A **50**, 475 (1978); H. Kronmüller, At. Energy Rev. Suppl. **1**, 255 (1981); H. Kronmüller, M. Fähnle, M. Domann, H. Grimm, R. Grimm, and B. Gröger, J. Magn. Magn. Mater. **13**, 53 (1979).

[34]Y. Obi, H. Fujimore, and H. Saito, Jpn. J. Appl. Phys. **15**, 611 (1976); M. Takahashi, T. Suzuki, and T. Miyazaki, *ibid.* **16**, 521 (1971); S. Tsukahara, T. Satoh, and T. Tushima, IEEE Trans. Mag. **14**, 1022 (1978).

[35]P. Eisenberger and G. S. Brown, Solid State Commun. **29**, 481 (1979); R. Frahm, R. Haensel, and P. Rabe, in *EXAFS and Near Edge Structure, Proceedings of the 1st International Conference,* edited by A. Bianconi, L. Incoccia, and S. Stipcich, Springer Series in Chemical Physics Vol. 27 (Springer, Berlin, 1983), p. 107.

[36]M. De Crescenzi, A. Balzarotti, F. Comin, L. Incoccia, S. Mobilio, and N. Motta, Solid State Commun. **37**, 921 (1981); J. Wong and H. H. Liebermann, J. Non-Cryst. Solids **45**, 195 (1981); Phys. Rev. B **29**, 651 (1984); A. Sadoc, D. Raoux, P. Lagarde, and A. Fontaine, J. Non-Cryst. Solids **50**, 331 (1982); G. S. Cargill, W. Weber, and R. F. Boehme, in *EXAFS and Near Edge Structure, Proceedings of the 1st International Conference,* (Ref. 35), p. 277; F. Schmückle, P. Lamparter,

and S. Steeb, Z. Naturforsch. Teil A **37**, 572 (1982); R. Frahm and B. W. Pfalzgraf, J. Phys. F **13**, L229 (1983); S. Mobilio and L. Incoccia, Nuovo Cimento **3**, 846 (1984); A. Defrain, L. Bosio, R. Cortes, and P. Da Costa, J. Non-Cryst. Solids **61&62**, 439 (1984); K. B. Garg, K. Jerath, H. S. Chauhan, and U. Chandra, Pramāna, J. Phys. **27**, 821 (1986); E. Zschech, W. Blau, V. K. Fjodoròv, and M. A. Sheromov, Nucl. Instrum. Methods Phys. Res. A **282**, 568 (1989); P. Lagarde, J. Rivory, and G. Vlaic, J. Non-Cryst. Solids **57**, 275 (1983), and Ref. 37.

[37]R. Haensel, P. Rabe, G. Tolkiehn, and A. Werner, in *Liquid and Amorphous Metals,* edited by E. Lüscher and H. Coufal (Sijthoff & Noordhoff, Alphen aan den Rijn, the Netherlands, 1980), p. 459.

[38]G. C. Chi and G. S. Gargill III, in *Experimental Meson Spectroscopy - 1974 (Boston),* edited by D. A. Garelick, AIP Conf. Proc. No. 21 (AIP, New York, 1974), p. 359; Y. Waseda, *The Structure of Non-Crystalline Materials* (McGraw-Hill, New York, 1980), p. 123–124 (Figs. 4-29 and 4-30).

[39]P. Kizler and S. Steeb, in *Proceedings of the 5th XAFS Conference* [Physica B **158**, 392 (1989)].

[40]P. J. Durham, J. B. Pendry, and C. H. Hodges, Solid State Commun. **38**, 159 (1981).

[41]B. K. Teo and P. A. Lee, J. Am. Chem. Soc. **101**, 2815 (1979).

[42]P. J. Durham, J. B. Pendry, and C. H. Hodges, Comput. Phys. Commun. **25**, 193 (1982).

[43]D. D. Vvendensky, D. K. Saldin, and J. B. Pendry, Comput. Phys. Commun. **40**, 421 (1986).

[44]J. B. Pendry, *Low Energy Electron Diffraction* (Academic, London, 1974); T. L. Loucks, *The Augmented Plane Wave Method* (Benjamin, New York, 1967).

[45]E. Clementi and C. Roetti, At. Data Nucl. Data Tables **14**, 177 (1974).

[46]See standard books on the quantum theory of scattering; e.g., L. S. Rodberg and R. M. Thaler, *Introduction to the Quantum Theory of Scattering* (Academic, New York, 1967), p. 43.

[47]A. Brenner, D. E. Couch, and E. K. Williams, J. Res. Nat. Bur. Stand. **44**, 109 (1950); J. Logan and M. Yung, J. Non-Cryst. Solids **21**, 151 (1976); H. Bestgen, in *Proceedings of the 5th International Conference on Rapidly Quenched Metals (RQ5)* (Ref. 5), p. 443.

[48]D. Meyer, Diploma thesis, Technical University of Dresden, 1991; Kizler (Ref. 21).

[49]A. Krolzig, G. Materlik, M. Swars, and J. Zegenhagen, Nucl. Instrum. Methods Phys. Res. **219**, 430 (1984).

[50]R. Frahm, Ph.D. thesis, University of Kiel, 1983; for an introduction into the theory, see, e.g., B. K. Teo, *EXAFS: Basic Principles and Data Analysis* (Springer, Berlin, 1986); or *X-Ray Absorption,* edited by D. C. Koningsberger and R. Prins (Wiley, New York, 1988).

[51]A. G. McKale, B. W. Veal, A. P. Paulikas, S. K. Chan, and G. S. Knapp, J. Am. Chem. Soc. **110**, 3763 (1988).

[52]N. Lustig, J. S. Lannin, D. L. Price, and R. Hasegawa, J. Non-Cryst. Solids **75**, 277 (1985).

[53]R. Frahm, R. Haensel, and P. Rabe, J. Phys. Condens. Matter **1**, 1521 (1989).

[54]T. Fujiwara, J. Phys. F **12**, 661 (1982).

[55]S. Ishida, S. Asano, and J. Ishida, J. Phys. F **17**, 475 (1987).

[56]A. Bianconi, M. Dell'Ariccia, A. Gargano, and C. R. Natoli, in *EXAFS and Near Edge Structure I, Proceedings of the International Conference,* edited by A. Bianconi, L. Incoccia, and S. Stipcich, Springer Series in Chemical Physics Vol. 27 (Springer, Berlin, 1983), p. 57; A. Bianconi, M. Dell'Ariccia, P. J. Durham, and J. B. Pendry, Phys. Rev. B **26**, 6502 (1982).

[57]P. Kizler (unpublished).

[58]J. M. Dubois, P. H. Gaskell, and G. LeCaër, Proc. R. Soc. London A **402**, 323 (1985).

[59]P. Lagarde, J. Rivory, and G. Vlaic, J. Non-Cryst. Solids **57**, 275 (1983); J. M. Dubois, Ph.D. thesis, University of Nancy, 1981; data are displayed also in P. Lagarde, Nuovo Cimento D **3**, 885 (1984).

[60]J. Swierczek, J. Zbroszczyk, S. Szymura, and B. Wysłocki, Solid State Commun. **65**, 935 (1988).